J Mater Sci (2009) 44:5189–5196
DOI 10.1007/s10853-009-3699-x

FERROELECTRICS

Ferroelectric domain switching dynamics with combined 20 nm and 10 ns resolution

Nicholas A. Polomoff · Ramesh Nath Premnath · James L. Bosse · Bryan D. Huey

Received: 30 April 2009 / Accepted: 19 June 2009 / Published online: 10 July 2009

Abstract High speed piezo force microscopy (HSPFM) is employed to investigate ferroelectric domain nucleation and growth of an exposed PZT film. Twenty nanometer spatial and 10 ns temporal resolution is achieved using a pump:probe methodology, allowing area switching and individual domain dynamics to be monitored. Two complementary investigations are performed, mapping switching in either a single 2 μm × 2 μm area for 4.2 V pulses with durations ranging from 20 to 60 ns, or for 10 ns pulses with amplitudes varying from −4 to −4.7 V. In this manner, nascent domains, as well as long-term growth, are efficiently quantified with substantial statistical significance due to the hundreds of images that can reasonably be acquired in a practical experimental session. The switching mechanism, areal switching rate, domain nucleation time, and domain wall velocity are each clearly independent of pulse width. In contrast, these parameters are strongly influenced by increasing pulse heights, including a faster switching rate, shorter nucleation times, and additional nucleation sites. This suggests a spatially and energetically heterogeneous landscape of activation energies for domain reversal sites, only some of which can therefore participate in switching with weak pulses but many of which are activated for strong pulses. These quantitative results, and the spatial, temporal, and statistical benefits provided by HSPFM combined with pump:probe techniques, have important implications for determining ultimate switching speeds, ideal device geometries, and optimal materials selection and processing.

N. A. Polomoff · R. N. Premnath · J. L. Bosse · B. D. Huey (✉)
Institute of Materials Science, University of Connecticut,
97 N. Eagleville Rd., Unit 3136, Storrs, CT 06269-3136, USA
e-mail: bhuey@ims.uconn.edu

Present Address:
R. N. Premnath
Materials Science Division, Argonne National Laboratory,
9700 S. Cass Ave., Building 221, Argonne, IL 60439, USA

Introduction

In order to improve ultimate switching speeds and reliability in storage devices, there is considerable interest in investigating switching dynamics at the nanoscale. For ferroelectrics, scanning probe microscopy (SPM) has been used extensively due to its sensitivity to domain orientation via piezo-actuation in a mode known as piezo force microscopy (PFM) [1]. To characterize dynamics with PFM, domain wall relaxation has been monitored as a function of time [2–5] or domain radii after applying single pulses of various amplitudes and durations [6]. Measuring domain sizes as a function of annealing temperature further has been used to calculate activation energies for growth mechanisms [7].

Experiments into domain dynamics using pump:probe schemes have also been reported, both for free surfaces, as well as through a top electrode in capacitor geometries [8–11], revealing individual domain nucleation and growth within the structure. The influence of edge effects on switching dynamics in microfabricated and FIB prepared film structures [12] have similarly been published [13, 14]. In these configurations, a voltage pulse is essentially applied to a capacitor structure, the stable domain pattern from this uniform field poling is imaged through the capacitor top electrode, and then these steps are repeated numerous times. This has allowed temporal resolution down to 20 ns in PFM [15], while domain wall velocities as high as 40 m/s have been mapped in similarly configured measurements using synchrotron-based, spatially resolved X-ray diffraction spectra instead of scanning probe microscopy [16].

This paper reports somewhat related experiments, but with two fundamental differences. First, ferroelectric thin films with exposed top surfaces are studied instead of capacitor structures. This allows individual domain switching to be monitored independent of adjacent features and without any influence of the top electrode interface, providing insight into the fundamental response of the thin film itself. Second, a high speed variation of PFM recently developed by the authors is employed [17]. This uniquely provides nanoscale images in seconds instead of minutes, such that the hundreds of images that can reasonably be acquired during a practical switching experiment yield both high temporal resolution and data over sufficiently long durations to track domain nucleation, growth, and impingement on adjacent domains. In this manner, switching mechanisms and kinetics can uniquely be mapped and statistically investigated even for nascent domains.

Experimental procedure

PFM is based on an atomic force microscope, configured with a conducting tip and cantilever in order to directly apply a bias to a piezoelectric sample at the contacting tip apex. The resulting electric field induces a surface displacement via the converse piezoelectric effect, which is simultaneously detected by the tip and highly compliant cantilever. AC fields are usually employed to leverage the enhanced signal to noise ratios possible using a lock-in amplifier (SRS 844), routinely providing picometer sensitivity. In the case of a ferroelectric, the phase of the piezoresponse is defined by the domain orientation, so that PFM phase images depict the distribution of domains. Here, epitaxial films are characterized, such that domain reversal obeys a 180° phase shift as sketched on the left of Fig. 1 for 4 line profiles as indicated. This mode is particularly useful for characterizing domain switching dynamics, as it easily allows the evolution of nucleating and growing domains to be mapped and computationally evaluated. If a DC bias is also superimposed on the AC signal so that the sum is sufficient to surpass the coercive field, orientation, and switching can be investigated simultaneously as described elsewhere [17]. Only an AC bias is applied here during imaging, however, and with an amplitude sufficiently less than the coercive voltage. Therefore, the domain orientation is not modified whatsoever during orientation mapping.

The high speed variation of PFM employed in this work (HSPFM) is achieved by coupling ultrasonic methods [18–21] with standard PFM [22]. This yields spatial resolution equivalent to standard PFM, but substantially enhances imaging speeds by up to several orders of magnitude as previously described by the authors [17]. This requires external high speed data acquisition (Measurement Computing DAS-4020), and employs high frequency electric fields in the MHz range instead of 1–300 kHz range as normally reported. For all results presented in this work, HSPFM line scanning rates of 40–80 Hz are employed. This equates to full resolution image acquisition in 3.2–6.4 s, compared to 4 min per frame or worse for standard AFM or PFM investigations.

For pump:probe experiments, one HSPFM frame is acquired while scanning in one direction as described above (the 'probe'). While scanning in the other direction, however, every image pixel is 'pumped' with a pulse of selectable amplitude and duration as sketched in the center of Fig. 1. The pulses are triggered by a pixel clock from the AFM system (Asylum Research MFP-3d) driving an external trigger for pulse application in a computer controlled Agilent 80 MHz arbitrary waveform generator (model 33250A). For a 2.56 μm × 2.56 μm image, with 256 pixel and line resolution, this amounts to 1 pulse every 10 nm, which is essentially the tip contact radius as 20 nm features are resolved in the images. Of course, more pulses could be applied per pixel, or pulses could be applied to only a subset of the pixels in the imaged area, but for these results any given area of the image is essentially pulsed once per pumping cycle, and then the outcome is imaged in the frame immediately following. In this manner, the generator is simply toggled between imaging and pulsing modes depending on the scan direction. These steps are repeated at least 80 times in a single location to allow

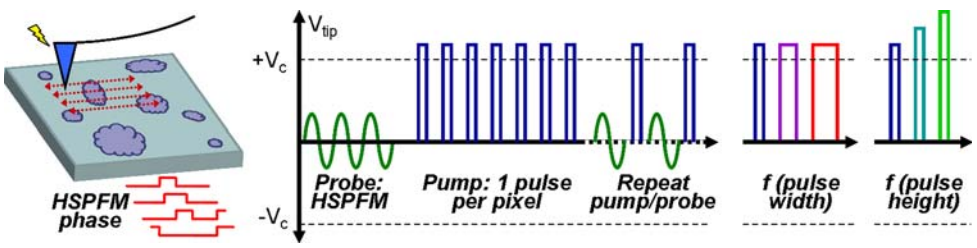

Fig. 1 Sketch of combined HSPFM and pump:probe measurement scheme, identifying the voltage applied directly to the tip while scanning with respect to the coercive potential for domain poling ($\pm V_c$) including pump (pulse) and probe (sinusoidal) cycles, measurements as a function of pulse width, and those as a function of pulse height

domain nucleation and growth to be sufficiently tracked for proper statistical analysis, a task that would require more than 5 h with normal PFM at a 1 Hz line rate but is completed in less than 8 min with HSPFM.

To practically analyze the hundreds of images which result, each image series (i.e., all images acquired under fixed pulsing conditions) is assembled into a movie. Domains are then automatically identified for each movie frame using a simple binary contrast threshold in standard image analysis software packages (both ImageJ and Improvision Volocity are utilized). This generates statistics for each temporal step in the switching process of any and all regions where contrast is present, i.e., domains, including their location, area, and perimeter (useful for arbitrarily shaped domains). Domains in sequential images at essentially the same area are then automatically linked for tracking as a function of time, and finally inspected visually to avoid misidentification. Domains at image edges are explicitly ignored since their extent of switching beyond the scanned area cannot be known. Once domains coalesce, they are no longer tracked, as this work focuses explicitly on independent domains.

In this manner, the influence of pulse shape on switching rates and mechanisms is uniquely investigated with high spatial and temporal resolution. Specifically, distinct pulse durations are first explored, including 20, 40, 50, and 60 ns square pulses, all with a uni-polar amplitude of +4.2 V (Fig. 1, right). Next, areas switched with different uni-polar amplitudes are characterized, including −4, −4.3, −4.5, and −4.7 V, all with a duration of 10 ns. The combined results are ultimately explained based on the energetic distribution of defects in the film.

The sample studied is a 30-nm thick Lead Zirconium Titanate (PZT) thin film, grown epitaxially on single crystal $SrTiO_3$ with an intermediate Strontium Ruthenate (SRO) back electrode. The film is provided by Y. H. Chu and R. Ramesh, UC Berkeley. The experimental geometry is the same as that presented previously by the authors [17].

Results

Influence of pulse duration

Figure 2 presents a montage of 40 individual 2 μm × 2 μm HSPFM phase images acquired during pump:probe measurements, assembled from more than 400 total images with equal temporal separation. Specifically, each column displays the progression of domain switching upon applying single 4.2 V unipolar pulses to all 256 × 256 pixels per image with distinct durations ranging from 20 to 60 ns (labeled at top). Since the pulse amplitude is beyond the coercive field, the domain distribution evolves in each

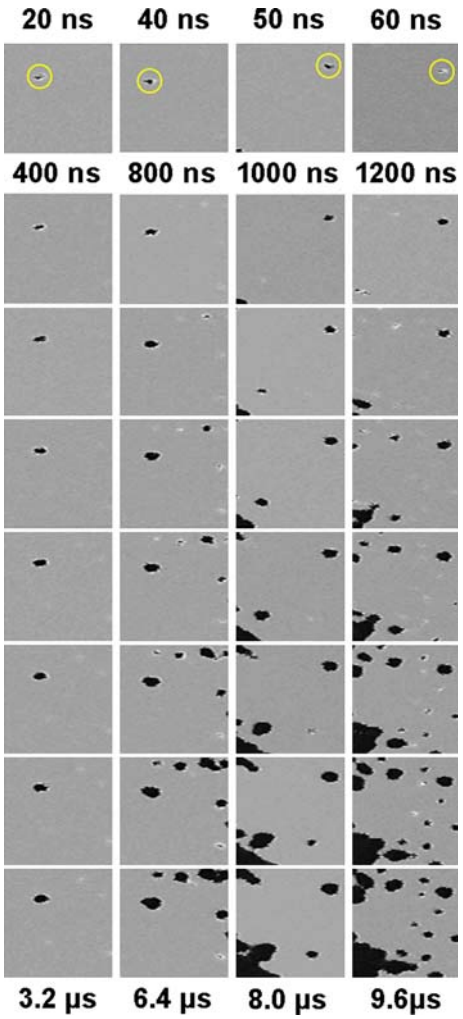

Fig. 2 Montage of 32 HSPFM phase images (2 μm × 2 μm) for each of 4 pulse durations (in *columns*) with increasing accumulated pulse times between each frame (labeled after *first row*) and overall (*top* to *bottom* as labeled at the *base*)

column, with more complete area switching by the final frames for the longer duration pulses (i.e., at right). Note that continuous HSPFM imaging without interspersed pulses, or images acquired following repeated sub-coercive-field pulses, do not change at all (not shown for brevity). The accumulated pulsing time between each frame shown is indicated after the first image row, while the final accumulated pulsing time for each series (column) is identified at the base of the figure. All scanning is performed in nearly the same area, except for experimental drift, with the same single domain initially nucleating for each of the pulse conditions (circled in the initial frames only). Before each series, the area is pre-poled with an oppositely oriented DC bias for uniform starting conditions.

For every image from the dataset summarized in Fig. 2, the percentage of overall switched area (i.e., the fraction of dark contrast) is easily determined. Plotting this as a

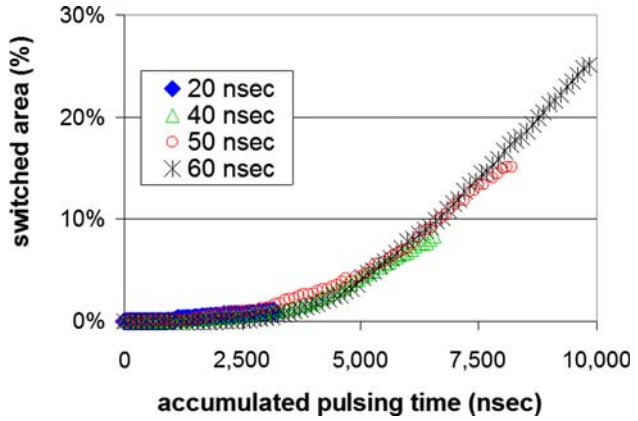

Fig. 3 Percent switched area as a function of pulse duration and accumulated pulsing time for the entire set of images that are partially summarized in Fig. 2

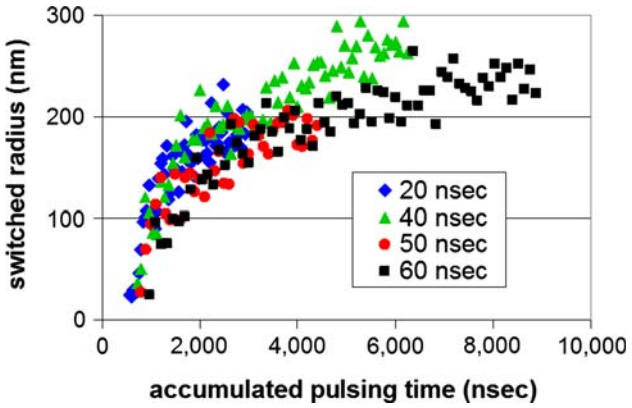

Fig. 5 Domain radius versus switching time for increasing pulse widths, all for a single identical domain identified by *circles* in the *top row* of each *column* of Fig. 2

function of accumulated pulsing time reveals areal switching rates for the various pulse durations (Fig. 3). The curves strongly overlap, suggesting that the switching is linearly proportional to pulse width. Note that implementing wider pulses, or imaging even more frames, eventually leads to the widely observed S-like behavior for switching in ferroelectric capacitor structures, but here the early stages of switching are emphasized so only the onset of the S-like behavior is captured.

Combining the overlapping trends in Fig. 3 with the visual results of Fig. 2, the switching mechanism itself seems uninfluenced by the pulse width. To confirm this, the number of domains per frame is recorded as a function of accumulated pulsing time (Fig. 4). Once again, data for the four distinct pulse widths essentially overlaps. Differences are attributed to spatial drift between measurement series, causing slightly different areas with different nucleation sites to be sampled.

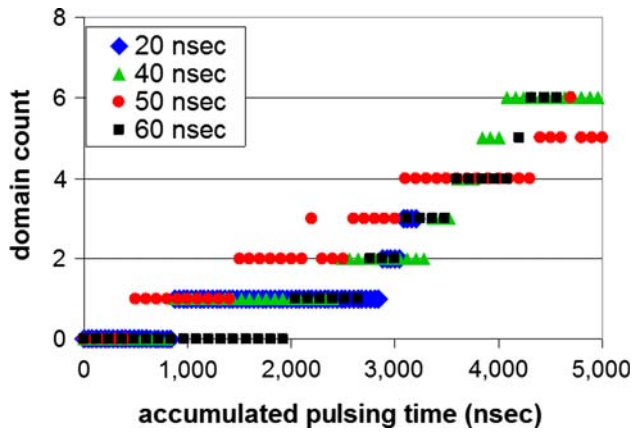

Fig. 4 Total number of distinct domains per image frame as a function of pulse width and accumulated pulsing time for Fig. 2

To fully discount spatial drift during the measurements, nucleation and growth for a single domain that appears in every pulse width series of Fig. 2 (circled) has been compared. The domain radius for this one domain is presented in Fig. 5 with respect to accumulated pulsing time for each pulse width employed, calculated by tracking the square root of the domain area for every image frame where this feature remains isolated. Three important observation results are as follows: First, the results overlap yet again for each pulse width considered, with the nucleation time and growth rates essentially the same within experimental scatter. Second, the domain appears to grow almost linearly beyond approximately 2000 ns, as observed elsewhere by the authors for similar, though non-pulsing, conditions [23]. Third, the extrapolated nucleation time (pulsing time for zero radius) is only approximately 600 ns, a value difficult to directly measure for individual features without the benefit of high temporal and spatial resolution afforded by HSPFM.

Practically, these results affirm that longer pulse widths in ferroelectric pump:probe measurements simply enable switching to be monitored more completely for a fixed number of imaging steps, and hence microscope use time. Short pulse durations, on the other hand, allow nascent domains to be efficiently monitored with high temporal resolution. Combining these characteristics has been employed elsewhere when implementing pulses of exponentially longer durations [15], which are especially useful to overcome standard PFM imaging speed limitations. Here, the higher speeds enabled by HSPFM preclude this limitation, but more importantly provide direct proof of the relatively negligible influence of pulse widths on areal and even individual domain switching mechanisms and dynamics. This is leveraged in the remainder of the paper, which measures the influence of pulse amplitude on domain switching by varying pulse heights for a fixed pulse width.

Influence of pulse amplitude

Figure 6 presents another montage of 2 μm × 2 μm HSPFM images, acquired based on 10 ns pulses per pixel with four distinct unipolar pulse amplitudes ranging from −4.0 to −4.7 V. As before, accumulated pulse times between each displayed frame are labeled after the first image row, and the total accumulated pulse time per parameter is listed at the base of the figure. Here, though, the columns display the evolution of domains for various pulse heights as labeled at the top of the figure. A substantially different behavior is obvious compared to Fig. 2, which considered different pulse durations instead of amplitudes. Qualitatively, the maximum number of domains seems to increase with the pulse amplitude. The imaged area also appears to switch in far fewer frames for stronger pulse amplitudes, even necessitating a much shorter time step between displayed frames for the highest amplitude (−4.7 V, though the pulse time between each collected image remained the same, 10 ns).

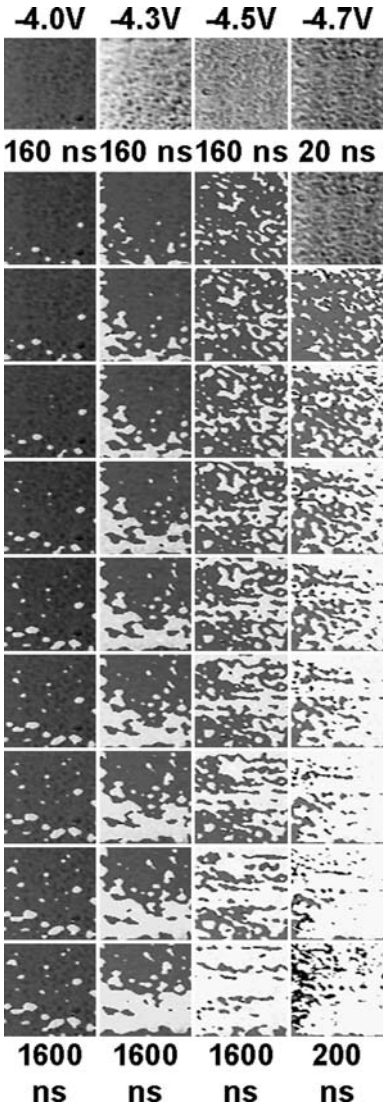

Fig. 6 Montage of 40 HSPFM phase images (2 μm × 2 μm) summarizing results for 4 pulse amplitudes (*columns*), with increasing accumulated pulse times between frames (labeled after *first row*) and overall (labeled at *base*, note fewer images are skipped between displayed frames for the strongest amplitude)

To quantify these observations, Fig. 7 presents the overall switched area for the various pulse amplitudes as a function of the accumulated pulse time. As before, this is based on a binary contrast threshold from all acquired images (260 total); necessarily, only a small subset of these are shown in Fig. 6. Switching progresses in just a few image frames with the strongest field (−4.7 V), polarizing nearly the entire image area in less than 300 accumulated nanosecond of 10 ns pulses. The weakest field (−4.0 V), on the other hand, barely completes 2% of areal switching in the same amount of time. Extrapolating this rate linearly, the full area would not completely switch until 13 μs of pulses are applied.

The benefit of stronger pulses for rapid switching response times is clear, though not surprising since areal switching rates have long been modeled with an exponential relationship to the applied field. Accordingly, Fig. 8 displays the calculated initial area switching rates from the slopes in Fig. 7 versus the potential, and the exponential curve fit is nearly perfect ($R^2 = 0.99$). The enhanced spatial and temporal resolution available with HSPFM, therefore, provides absolute confirmation of the exponential relationship between pulse height and switching rates at the nanosecond and nanometer scales.

A plot of the number of domains versus accumulated pulsing time, Fig. 9, is also drastically different from the counterpart measurement for pulse width, Fig. 4. Initially, there are far more domains for higher switching amplitudes. This is partially because nucleation and growth rates increase exponentially with pulse height, so that any given

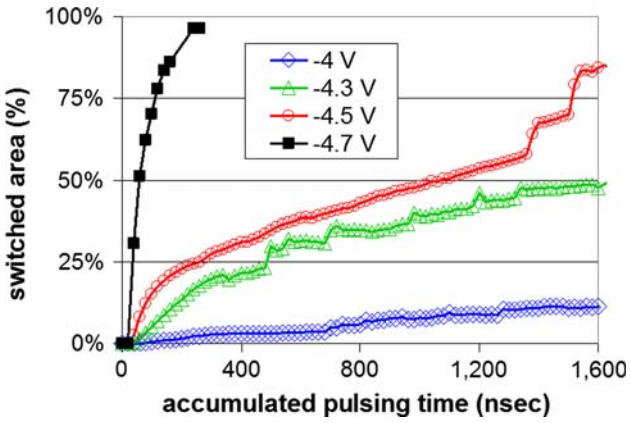

Fig. 7 Percent switched area as a function of pulse height and accumulated pulsing time from the entire set of images summarized in Fig. 6

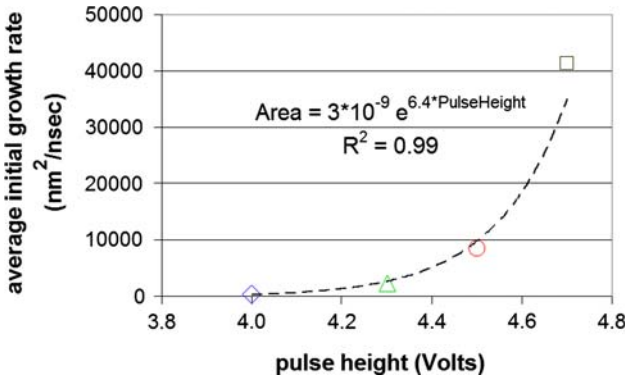

Fig. 8 Average initial growth rate for areal switching as a function of pulse height, from Fig. 7

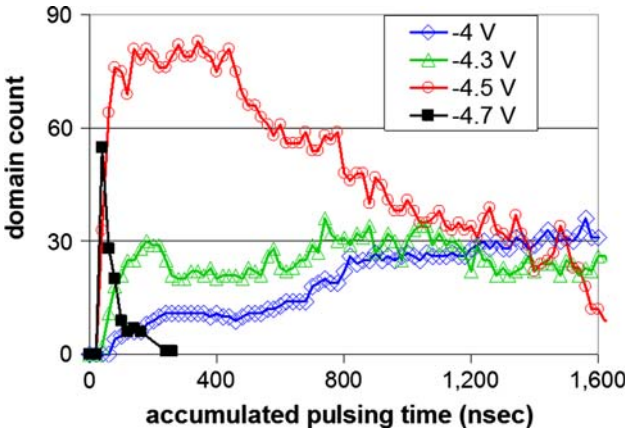

Fig. 9 Number of distinct domains per image frame versus accumulated pulsing time for various pulse heights, from Fig. 6

domains are simply detectable after less poling time. Additionally, however, visually comparing images from different voltages suggests that a much greater density of nucleation sites also participate in areal switching for strong pulses. This leads to a sharp peak in the domain count with −4.7 V, which is predicted to be even higher if better temporal resolution could be achieved. This peak then diminishes as the numerous nucleated domains impinge on one another and are no longer tracked as individual features. For −4.5 V, a similar behavior is observed, though fewer domains are identified and they persist longer before combining with neighbors. For −4.0 V the number of domains per image was still growing when the experiment was terminated. In comparison, the pulse width experiment revealed essentially the same domains for each series, which simply appeared (i.e., nucleated) in earlier or later image frames depending on the applied pulse width. These contrary observations strongly suggest a heterogeneous landscape of individual activation energies for possible domain nuclei. Only the lowest energy sites are activated with low pulsing potentials, limiting the domain count and generally slowing the poling process. But for higher amplitude pulses, sufficient energy is provided that many more domains are activated in the same amount of pulsing time, substantially accelerating areal switching.

Considering domain nucleation more carefully, tracking the essentially linear growth of individual domains from Figs. 2 and 6, and extrapolating back to the time axis, allows their discrete nucleation times to be calculated as described previously by the authors [23]. Figure 10 plots histograms of these measured nucleation times, both for the pulse width (a) and pulse height (b) investigations. When varying pulsing times only, the nucleation time is predicted and observed not to vary, excepting that some domains with very short nucleation times may not be discretely captured by the longer pulse widths (essentially they grow together, or to an image edge, too quickly to independently discern and therefore to properly include in the statistics). Varying pulse heights, on the other hand, should exhibit more rapid nucleation times and more sites for high potentials, and broader distributions of nucleation times as well as fewer sites for lower potentials, as observed.

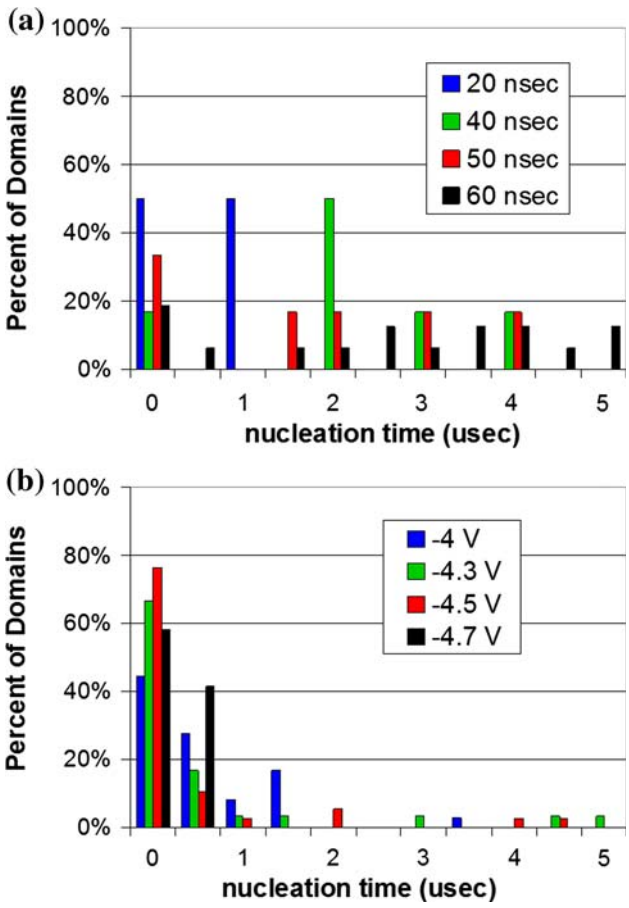

Fig. 10 Histogram of nucleation times (500 ns bins) displayed as a percentage of all domains independently identified for **a** increasing pulse widths and **b** increasing pulse heights

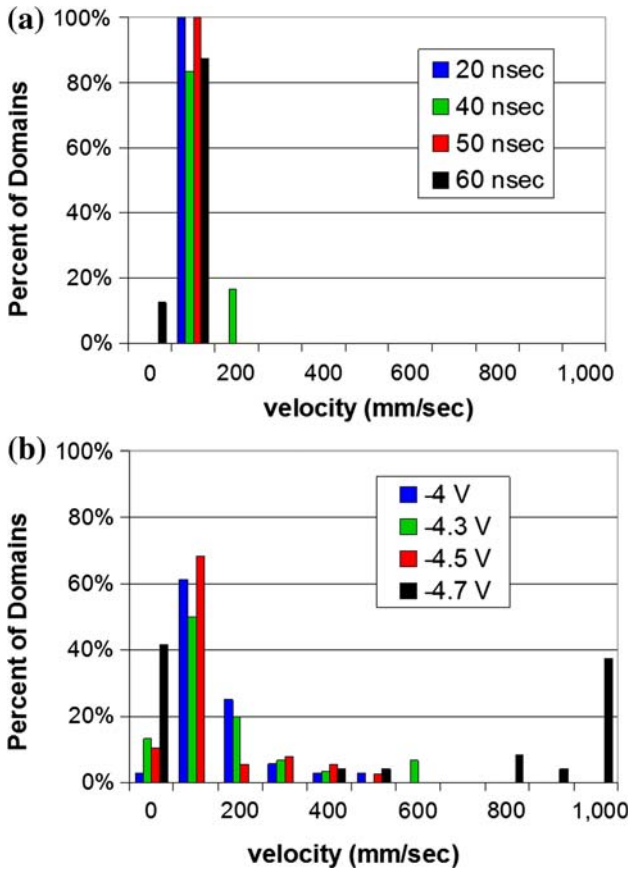

Fig. 11 Histogram of domain wall velocities (100 mm/s bins) as a percentage of all domains independently identified for **a** increasing pulse widths and **b** increasing pulse heights

Figure 11 displays histograms for the velocities of individual domains as well, similar to Fig. 10 except these plots are determined from the areal growth slopes for distinct switching sites. Again as anticipated, pulse width is essentially irrelevant to the domain wall velocity (a). Separately, for weak pulse amplitudes, the domain velocities should be relatively slow, with the histogram peak shifting to higher velocities for stronger pulses just as observed (b).

These results agree well with the reasonable assumption that there is a distribution of nucleation sites in any given ferroelectric thin film, both spatially and energetically. The activation energies for these distinct features will be a function of defect type, depth, clustering with other nearby defects, etc. Measurements at a given potential thereby activate only those nucleation sites with an appropriately low activation energy, regardless of pulse width. Conversely, for increasing pulse heights all domains with low activation energies will still nucleate, but higher energy defects will also develop and additionally contribute to area switching. Performing multiple measurements with different pulse amplitudes, therefore, provides a means to map not only the spatial distribution of defects, but also their relative energies.

Finally, the curves of Figs. 3 and 7 exhibit the familiar exponential 'S-curve' behavior often seen in macroscopic ferroelectric switching measurements, usually acquired by monitoring polarization as a function of time through electrodes in a parallel-plate or interdigitated capacitor geometry. Such measurements are generally analyzed following the KAI model [24–26], culminating in an average activation energy for switching for the device area. An important outcome of the HSPFM measurements reported here is therefore that while areal polarization can be recorded, the switching is also visualized locally. As a result, the actual underlying switching mechanisms can clearly be distinguished (nucleation vs. growth dominated, for example) as a function of sample composition, materials processing, device geometry, etc. Necessarily separate works analyzing this point in greater detail are underway, in terms of the local activation energies, as well as direct comparisons between nanoscale and macroscopic S-curve behavior.

Conclusion

Ferroelectric domain switching is uniquely investigated for various poling pulse amplitudes and durations by combining a pump:probe scheme with HSPFM. In such experiments, an area is alternately biased with voltage pulses, and imaged with high speed PFM, efficiently providing hundreds of property maps that reveal the dynamics of local domain reversal with down to 20 nm spatial and 10 ns temporal resolution. In terms of pulse duration, the pulse width is shown to be insignificant with respect to polarization dynamics. This validates the pump:probe scheme in general for PFM, and is useful in guiding future experiments focusing on both nascent as well as mature domain dynamics. Pulse amplitude, on the other hand, is statistically found to both exponentially increase areal switching rates, as well as strongly influence individual domain dynamics, including nucleation times, growth velocities, and densities of switched domains. This evidence, uniquely afforded by the high speed technique, supports a heterogeneous landscape of activation energies (spatially and energetically) for domain nucleation and growth. Low energy sites are easily nucleated, while high energy sites are only activated if sufficient voltage is applied; otherwise, they essentially do not participate in areal switching. Such effects vary as a function of the ferroelectric material, processing, geometry, switching cycles, and so on, and have a profound influence on ultimate switching speeds, domain stability, etc., establishing HSPFM-based measurements as a powerful tool for future ferroelectric device or process optimization.

Acknowledgements This work is partially supported by a high speed SPM development award from the National Science Foundation, Instrumentation for Materials Research, #0817263. Materials were provided by R. Ramesh, U.C. Berkeley Department of Physics, and Y. H. Chu, National Chiao Tung University Department of Materials Science and Engineering, HsinChu, Taiwan.

References

1. Gruverman A, Kalinin S (2006) J Mater Sci 41:107. doi: 10.1007/s10853-005-5946-0
2. Nagarajan V, Aggarwal S, Gruverman A, Ramesh R, Waser R (2005) Appl Phys Lett 86:262910
3. Ganpule CS, Roytburd AL, Nagarajan V et al (2002) Phys Rev B 65:014101
4. Paruch P, Giamarchi T, Triscone JM (2005) Phys Rev Lett 94:197601
5. Roelofs A, Bottger U, Waser R, Schlaphof F, Trogisch S, Eng LM (2000) Appl Phys Lett 77:3444
6. Tybell T, Paruch P, Giamarchi T, Triscone JM (2002) Phys Rev Lett 89:097601
7. Jo JY, Yang SM, Kim TH et al (2009) Phys Rev Lett 102:045701
8. Hong S, Colla EL, Kim E et al (1999) J Appl Phys 86:607
9. Kim DJ, Jo JY, Kim TH et al (2007) Appl Phys Lett 91:132903
10. Yang SM, Jo JY, Kim DJ et al (2008) Appl Phys Lett 92:252901
11. Gruverman A, Rodriguez BJ, Dehoff C et al (2005) Appl Phys Lett 87:082902
12. Hambe M, Wicks S, Gregg J, Nagarajan V (2008) Nanotechnology 19:175302
13. Gruverman A, Wu D, Fan H et al (2008) J Phys: Condens Matter 20:342201
14. Hong S, Klug J, Park M et al (2009) J Appl Phys 105:061619
15. Gruverman A, Wu D, Scott JF (2008) Phys Rev Lett 100:097601
16. Grigoriev A, Do D-H, Kim DM et al (2006) Phys Rev Lett 96:187601
17. Nath R, Chu YH, Polomoff NA, Ramesh R, Huey BD (2008) Appl Phys Lett 93:072905
18. Hurley DC, Kopycinska-Muller M, Kos AB, Geiss RH (2005) Meas Sci Technol 16:2167
19. Kolosov OV, Castell MR, Marsh CD, Briggs GAD, Kamins TI, Williams RS (1998) Phys Rev Lett 81:1046
20. Rabe U, Scherer V, Hirsekorn S, Arnold W (1997) J Vac Sci Technol B 15:1506
21. Yin Q, Zeng H, Yu H, Li GR (2006) J Mater Sci 41:259. doi: 10.1007/s10853-005-7244-2
22. Huey BD (2007) Annu Rev Mater Res 37:351
23. Polomoff NA, Nath R, Bosse JL, Huey BD (2009) JVST B 27:1011
24. Dimmler K, Parris M, Butler DE, Pouligny SB, Scott JF, Ishibashi Y (1987) J Appl Phys 61:5467
25. Jo JY, Han HS, Yoon JG, Song TK, Kim SH, Noh TW (2007) Phys Rev Lett 99:267602
26. So Y, Kim D, Noh T, Yoon J, Song T (2005) Appl Phys Lett 86:092905